Study on water flow field around a stationary air bubble attached at the top wall of a circular pipe

C. Lin[1], C. H. Lu[1], J. Yang[2] & T. Liu[2]
[1]*Department of Civil Engineering, National Chung Hsing University, Taiwan*
[2]*Hydraulic Design and River Engineering, KTH, Stockholm, Sweden*

Abstract

The presence of bubbles in a pipeline is thought to be one of the reasons to cause the hydraulic-electrical and hydraulic-mechanical facility systems to lose their efficiency. From previous research, the bubble also reduces the effective pipe cross section, which results in a reduction in pipe capacity. The efficiency and service life of pumps and turbines are reduced and shortened consequently. It may even create the interruption of the flow field within blowout phenomenon. As a result, the presence of a bubble in the pipeline is anticipated to create potential hazards. Therefore, it is very interesting to make clear the corresponding variation of a water flow field around a stationary air bubble attached at the top inner-wall of pipe due to *the surface problems in contact mechanism of these three phases among the solid wall of pipe, stationary air bubble, and ambient water flow*.

This study applied flow visualization techniques and high time-resolved PIV to investigate the characteristics of a flow field around a stationary bubble in a fully-developed horizontal pipe flow. Experiments were carried out in a pipe having a constant inner diameter of 9.60 cm and a length of 260.0 cm, yet varied with different bubble volumes (or lengths). Two settling water chambers with different still water levels were connected to both ends of the circular pipe. Titanium dioxide powder being uniformly dispersed in the pipe flow was used as a tracer both for flow visualization tests and for PIV measurements.

The results show that a horseshoe vortex and reverse flow at the upstream and downstream of the bubble respectively are commonly seen in all test cases. The experimental results also show that the shape and volume of a bubble highly

WIT Transactions on Engineering Sciences, Vol 79, © 2013 WIT Press
www.witpress.com, ISSN 1743-3533 (on-line)
doi:10.2495/MPF130271

affect the flow field in the surroundings of the stationary air bubble. Since the bubble surface is slippery, flow velocity exists on the surface of a bubble. As a result, the reverse flow at the end of a long-flat bubble would not affect the velocity on the bubble surface.

Keywords: air pocket, particle image velocimetry, shear layer, slippery motion, characteristic length (or velocity) scale.

1 Introduction

The existence of air bubbles in pressurized systems of water supply or hydropower plants (e.g., pipeline or bottom spillway) causes negative influence on the efficiency and operation cost. It is often regarded as one of the main reasons to make the hydro-electrical and hydro-mechanical systems malfunction, eventually jeopardizing the operational safety of these systems. In addition, the presence of air bubbles stuck at the top wall of a horizontal or downward-inclined pipe reduces the effective pipe cross section, resulting in a reduction in pipe transport capacity.

An experimental study on the motion of long bubbles in closed tubes was made by Zukoski [1], in which the influence of viscosity of water, the surface tension of air bubble, and inclination angle of pipe were considered. Bendiksen [2] investigated experimentally the relative motion of single long air bubble suspended in a liquid flow in tilting pipe, aiming to determine the effect of pipe inclination on bubble motion, using liquid Reynolds and Froude numbers, and pipe diameter as the indicative parameters.

Lauchlan *et al.* [3] provided the state-of-the-art illustration in a literature review concerning the air in pipelines. They not only summarized typical flow patterns for either vertical or horizontal flow, as mentioned by Falvey [4] and Rouhani and Sohal [5], in a pipe system; but also pointed out that these patterns vary depending on the relative proportion of air and water as well as the slope of pipeline. Little [6] then performed tests on the air pockets in pipe diameter of 15.0 cm with a slope varying from zero to 22.5° downwards in the flow direction. He found that air pockets were distinct from small air bubbles because air bubbles would likely to be easily moved, but may tend to agglomerate into air pockets.

Furthermore, Wickenhauser and Kriewitz [7] presented the experimental investigation of air transport in a continuous two-phase, air-water flow in downward inclined large pipes with inclinations between 0.004 and 0.087. They reported several items including the flow pattern, bubble shape, and air transport capacity in continuous air-water flow. Recently, Liu and Yang [8] measured the critical velocity, which is the minimal water velocity to start moving an air pocket, in a pipe with an inner diameter of 24.0 cm and an inclination of 18.2°. Their results showed that the critical velocity in the rough pipe was independent of the air-pocket volume; and in the smooth pipe it did not increase with increasing pipe diameter as much as those indicated by previous researchers (e.g., Lauchlan *et al.* [3] and Estrada [9]). The authors also pointed out that pipe

roughness did not affect the moving velocity of air-pocket when it moved upstream in an 18.2° downward-inclined pipe.

Based on the literature review, it can be found that experimental investigation on velocity field of water around moving or stationary air-pockets, even for the simplest case of only an air-pocket adhered to the inner top-wall of either horizontal or inclined pipe is still very rudimentary. Accomplishment of this kind of investigation not only enhances our understanding in such complex flow and sheds promising light on the un-clear mechanism underlying the flow, but also can be used as a useful data bank for validation of future numerical studies. In the present study, flow visualization technique and high-speed particle image velocimetry (HSPIV) were used to investigate the characteristics of velocity field of water flow field around an air bubble (or pocket) attached at the top wall of a fully-developed, horizontal pipe.

2 Experimentation

The experiments were conducted in a horizontal transparent Plexiglas pipe, having a length of 260.0 cm and an inner diameter of 9.6 cm. The pipe was installed inside a glass-walled and glass-bottomed water channel at the Department of Civil Engineering, National Chung Hsing University. The total length of the water channel is 446.0 cm with a test section of 250.0 cm long, 25.0 cm wide, and 50.0 cm high. In order to generate the pressurized flow through the pipe, two vertical plates each with one hole (having the diameter a little larger than that of the pipe and aiming to support the pipe) were placed near the inlet and outlet ends of the pipe to stop the flow passing through the test section of water channel. Two settling water chambers with different still water levels were connected to the inlet and outlet ends of the pipe. The schematic diagram of the layout of experiment is shown in Figures 1(a), (b). A 4 HP pump was installed in between two stainless circular conduits each connecting with one water chamber and was used to drive the flow through the pipe. A honeycomb-like flow regulator made of many straws was placed perpendicularly to the axis of the pipe and right at the pipe entrance in order to remove large-scale irregularities and smooth the inlet flow.

In order to achieve the fully developed boundary layer flow in the pipe with a length of 260.0 cm, a tripping consisting of two strips of circumferential spikes was installed 15.0 cm downstream of the pipe inlet and used to enhance the growth of turbulent boundary layer thickness along the pipe. The circumferential spikes of the first and second strips all have heights of 1.0 cm and 0.5 cm, respectively. The center-to-center spacing of two neighboring spikes is 2.0 cm.

Air pocket was introduced from the outlet end into the top wall of the pipe at a certain position of interest by injecting air with syringe, which was connected with a long stainless steel tube having a length of about 200.0 cm and the outer and inner diameters of 2.0 mm and 1.5 mm, respectively. The air-pocket volume, V, can be easily measured via the indicator shown in the syringe injector. The sizes of the air pocket may vary with different bubble volume ranging from 1.0 ml to 10.0 ml.

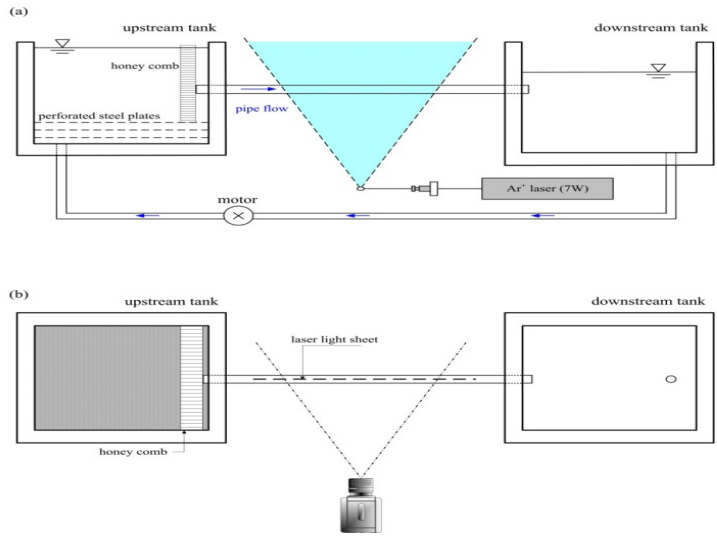

Figure 1: Schematic diagram of experimental layout for flow visualization test and HSPIV velocity measurement (a) side view; (b) top view.

The flow structure around the air pocket was visualized using particle trajectory technique. Water in the pipe and two chambers was mixed with titanium dioxide particles of mean diameter 10 μm for illumination under laser light. A 5 W argon-ion laser (Coherent Innova-90) was employed as a light source; laser beam was reflected by a glass cylinder of 0.57 cm diameter and spread into a fan-shaped light sheet of 1.0 mm thick. An image recording system, which is a 10-bit Complementary Metal-Oxide Semiconductor (CMOS) high-speed digital camera (Phantom V5.1) with resolution of 1,024 × 1,024 pixel and 1,200 Hz maximum framing rate, was used to capture particle-laden images of the water flow field.

A high-speed particle image velocimetry (HSPIV) system was used to measure the two-dimensional velocity fields of water flow in the surroundings of air pocket adhered to the inner top-wall of the horizontal pipe. The illumination method and tracing particles were the same as those employed in the flow visualization test. Velocity field of water flow around the air pocket was determined by cross-correlation analysis. A multi-grid interrogation process starting at 64 × 16 pixels and ending at 16 × 4 pixels (0.73 mm × 0.18 mm) with 50% overlap between adjacent sub-windows was used in the general calculation process.

The experimental conditions are listed in Table 1, in which the volume of air pocket V, the cross-sectional streamwise mean velocity U, the diameter of the pipe D are all identified. The Reynolds number Re (= UD/ν) based on the cross-sectional mean streamwise velocity U and the pipe inner diameter D, is kept at 17,100, showing the flow is actually of turbulent even without installing the spike-like tripping near the inlet of the pipe.

Two coordinate systems are used in the present study. The origin of the first coordinate system (X, Y) is right located at the top wall of pipe inlet with X being directed downstream and Y being the distance measured from the top wall of pipe toward the pipe center. The origin of the second coordinate system (x, y) is exactly located at the intersection point of the top wall of pipe and the line passing through the leading edge of air pocket and perpendicular to the top wall of pipe. The coordinates x and y herein represent the streamwise and transverse directions, respectively, with x being directed downstream positively and y being defined same as Y.

Table 1: A list of the experimental conditions.

Case	θ	V (ml)	U (cm/s)	D (cm)	$R_e = UD/v$
A	0°	1	17.8	9.6	17,100
B	0°	5	17.8	9.6	17,100
C	0°	10	17.8	9.6	17,100

3 Preliminary test for relationship between size and volume of air pocket

Variation of the sizes of air pocket adhered to the top wall of the pipe with the volume of air pocket is illustrated in this section. Note that the air pocket was injected from the syringe connected with a small stainless steel tube being introduced into the horizontal pipe. The sizes of air pocket, including the maximum height d_{max}, the length L, and the maximum width W_{max} can be

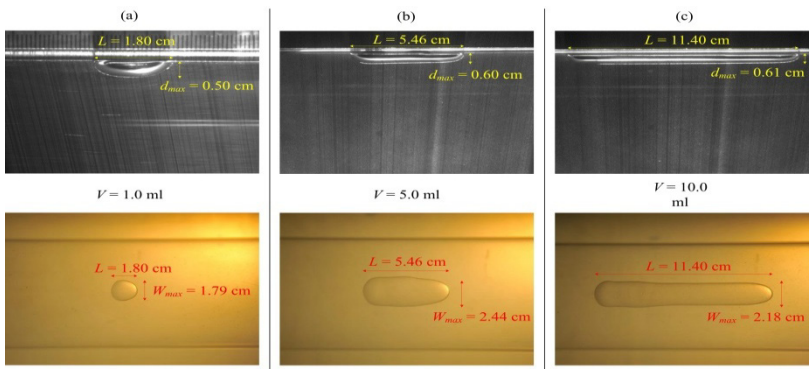

Figure 2: Serial photos show the sizes (including the maximum height d_{max} and the maximum width W_{max}, and the length L) of air pocket for its volume varied from 1.0 ml to 10.0 ml for a horizontal pipe. Note that the upper and lower photos were taken from the side and top views, respectively, and have different length scales.

determined by flow visualization pictures taken from the top and side views, respectively. Figures 2(a)–(c) demonstrate the pictures showing the sizes of air pocket in each photo with the air-pocket volume being changed from 1.0 ml to 10.0 ml in the horizontal pipe. From these three pictures taken from the top view, it can be found that the shape of the air pocket is fairly symmetrical with respect to the plane of symmetry (i.e., the vertical plane passing through both the center of the pipe and the central part of air pocket).

Because the air pocket injected into and stuck to the top wall of pipe is subjected to the shear force which is exerted by the viscous wall-shear and turbulent Reynolds stress, the air bubble is likely to be deformable which may depend on the volume of air pocket if the Reynolds number R_e is kept unchanged. Following the observational results as illustrated in Figures 2(a)–(c), Figure 3 shows subsequently the relationship of the air-pocket sizes with the variation of volume of air pocket in the horizontal pipe. It is very interesting to note that the variation of maximum height d_{max} and maximum width W_{max} of air pocket with air-pocket volume V is insignificant for V approximately larger than 2.0 ml; and that the air-pocket length L increases approximately linearly with an increase in the air-pocket volume for V ranging from 0 to 10.0 ml. That is to say that the increase in air-pocket volume has the prominent influence on the elongation of air-pocket while its effect is negligible on the maximum height and maximum width of air-pocket for $V > 2.0$ ml with the Reynolds number R_e and inclination angle (herein being equal to zero) being kept unchanged.

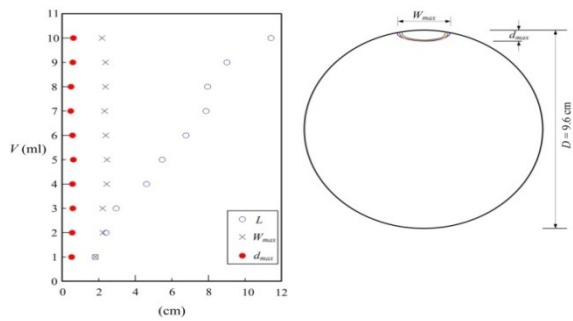

Figure 3: Variation of the sizes with the volume of air pocket in the horizontal pipe.

4 Results and discussions

4.1 Flow visualization results

Figure 4 represents one of the pictures of flow visualization on the instantaneous water flow field around a stationary air pocket with a volume of 1.0 ml in the *horizontal* pipe at R_e = 17,100 (Case A). The corresponding temporal variation in the water flow field around the air pocket can be clearly evidenced from the

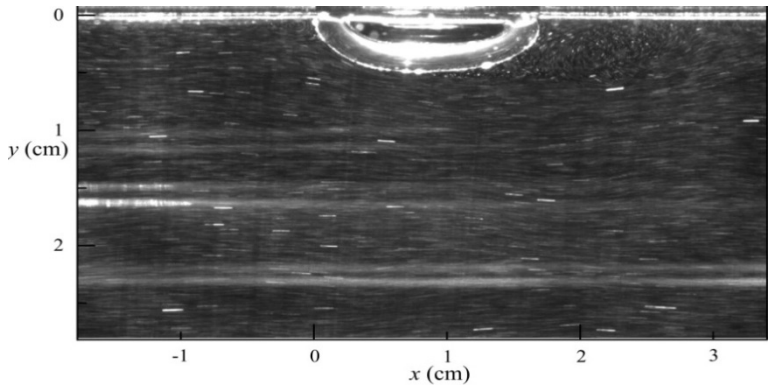

Figure 4: Flow visualization result of the instantaneous water flow field around a stationary air pocket having a volume of 1.0 ml in the horizontal pipe at R_e = 17,100 for Case A.

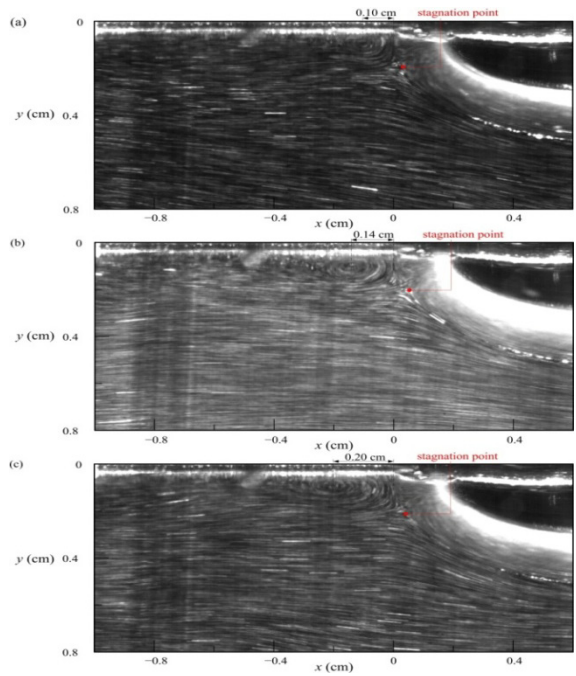

Figure 5: Three flow-visualized images depict different positions of core of horseshoe vortex oscillating upstream and downstream randomly for Case A.

pathline images continuously recorded by the high speed digital camera, demonstrating the water flow field is of quasi-steady. Figures 5(a)–(c) not only show obviously that horseshoe vortex is generated near the top wall at the upstream side of the leading edge of air pocket; but also reveal that, right at the (instantaneous) *stagnation point* where the water flow bifurcates on the air-pocket surface near its leading edge for Case A. Note that the vortical structure and core of horseshoe vortex oscillate upstream and downstream randomly with respect to a mean position.

In addition, more interesting phenomena can be also witnessed in Figures 6(a)–(c) for Case A, showing that exactly at the (instantaneous) *separation point* where the water particle moves away from the air-pocket surface. Fairly prominent formation of the shear layer then takes place right downstream of the (instantaneous) separation point located on the air-pocket

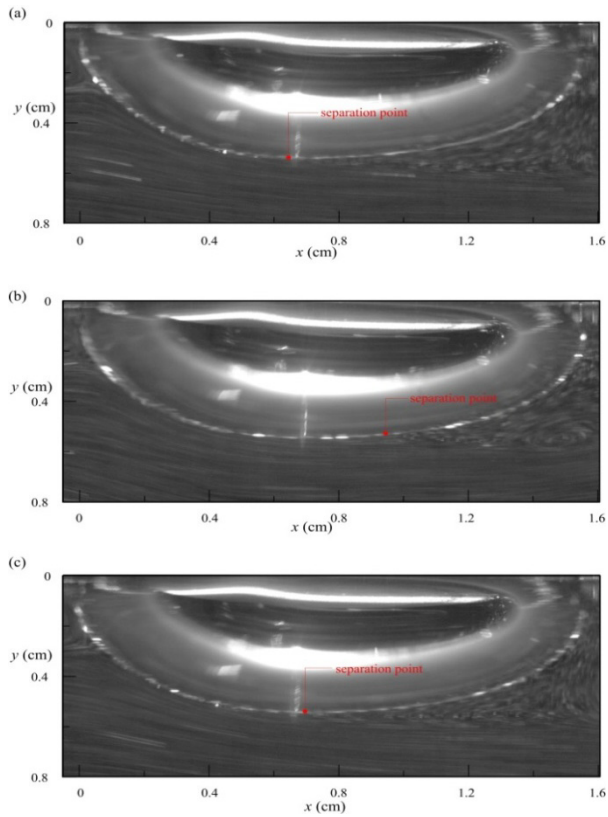

Figure 6: Three flow visualization images show that the separation point occurring at distinct positions on the air-pocket surface and the edge of shear layer being swinging upwards and downwards irregularly for Case A.

surface. It can be easily identified that the reverse flow occurs beneath the air pocket as well as at both upstream and downstream sides of the trailing edge of air pocket. Note that the position of separation point varies with time and the edge of shear layer may swing upwards and downwards irregularly due to the deformation (in the streamwise and vertical directions) of the air pocket being submerged in a fully-developed turbulent boundary layer flow in the pipe.

Furthermore, according to the flow observation from the animation pictures captured using high speed digital camera, it is surprisingly found that water particle moves right on the surface of air pocket since the air-bubble surface is slippery, where the traditional non-slip condition is no longer applied. In the plane of symmetry, the movement of the water particles right on the air-bubble surface is directed from the trailing edge of air pocket, then along the central part upstream, and finally to the (instantaneous) separation point where the water particle moves away from the air-pocket surface into the separated shear layer, as evidently witnessed in Figures 6(a)–(c) at R_e = 17,100 for the same Case A.

4.2 Velocity measurement results obtained by HSPIV

In the following, the water flow field and the velocity profiles measured by HSPIV are serially introduced. At first, the experimental results of Case A are used as an illustrating example. Figure 7 shows the mean velocity field of water flow around the stationary air pocket. In other words, Figure 7 clearly

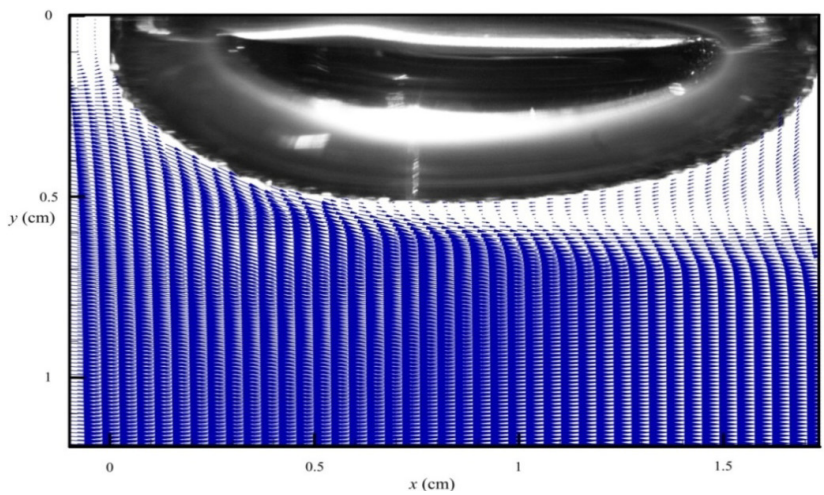

Figure 7: The mean velocity field of water flow is depicted especially for the region nearby around the stationary air pocket for Case A.

demonstrates three distinct flow regions: the horseshoe vortex taking place upstream of the air pocket and the stagnation point occurring on the air-pocket surface on its leading edge, formation of shear layer downstream of the separation point and reverse flow region right beneath the air pocket, and generation of wake flow downstream of the air pocket, respectively. Note that the flow structures shown in Figure 7 represents the corresponding characteristic of time-averaged result; however, those illustrated from flow visualization images shown in from Figure 4 to Figures 6(a)–(c) provide the instantaneous futures changing with time.

Figures 8(a)–(l) show the distributions of mean streamwise velocity, $u(y)$, measured at twelve streamwise positions extending from $x = -0.41$ cm (where the section is located upstream of the mean position of the core of horseshoe-vortex) to $x = +2.18$ cm (where the section is located downstream of the air pocket) at $R_e = 17{,}100$ for Case A. From Figure 8(a) and the counterparts obtained for -1.50 cm $< x < -0.51$ cm (not shown), we can find that the mean streamwise velocity close to the pipe top-wall, say $y < 0.10$ cm, is nearly equal to zero due to the obstruction of air pocket stuck to the top wall of the pipe; and that for $y > 0.11$ cm the mean streamwise velocity increases with the increase in y and reaches the maximum velocity u_{max} at the pipe center. Figure 8(b) illustrates the mean streamwise velocity profile measured at $x = -0.19$ cm and shows the trend globally similar to that shown in Figure 8(a), except within a thin layer with tiny reverse flow around $y = 0.09$ cm which is generated by the mean motion of the rotational horseshoe vortex with the mean position of the core. In addition, the mean streamwise velocity distribution obtained right at the leading edge of air pocket (i.e., $x = 0$ cm) is presented in Figure 8(c), in which for $y <$ 0.05 cm zero velocity occurs due to the existence of the leading edge of air pocket; and for $y > 0.10$ cm the mean streamwise velocity increases with the increase of y and also attains the maximum velocity u_{max} at the pipe center. Note that the velocity distribution shown herein for $x = 0$ cm fairly exhibits the future of traditional shear-layer profile having two different uniform streams with prominent velocity gradient in between.

Subsequently presented in Figures 8(d)–(g) are the distributions of mean streamwise velocity measured right beneath the air pocket at sections being located at $x = +0.15$ cm, $+0.32$ cm, $+0.45$ cm, and $+0.62$ cm, respectively. Note that in Figures 8(d), (e) the mean streamwise velocity measured at positions of $(x, y) = (0.15, 0.37)$ cm and $(0.32, 0.46)$ cm being nearly on or extremely close to the surface of air pocket is neither zero nor a tiny value, but about 10.0–9.0 cm/s, respectively, due to the slippery surface of the air bubble; and that the mean streamwise velocity also increases with increasing y for $y > 0.37$ cm and for $y >$ 0.46 cm, respectively. It is also worth of mentioning that the distribution of mean streamwise velocity obtained at the section of $x = +0.45$ cm as shown in Figure 8(f) exhibits very prominent velocity gradient between $y = 0.48$ cm (on which the surface of air pocket is located) and 0.58 cm (which is only about 0.1 cm beneath the surface of air pocket). According to the above-mentioned magnitudes of the mean streamwise velocity measured nearly on the surface of air pocket, it is very interesting to explore that the mean streamwise velocity

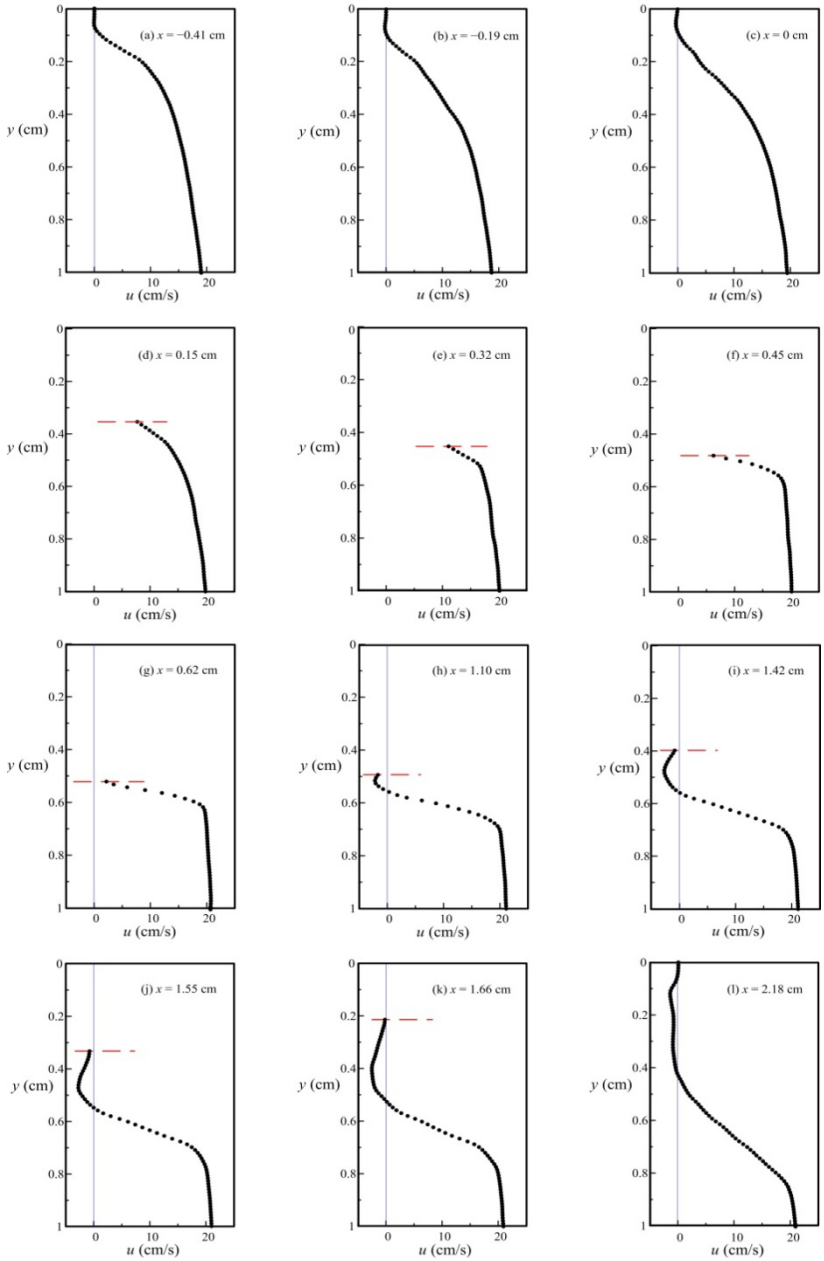

Figure 8: Distributions of the mean streamwise velocity measured at twelve streamwise positions extending from $x = -0.41$ cm to $x = +2.18$ cm.

nearly on the air-pocket surface becomes smaller while sections being varied from x = +0.15 cm to x = +0.45 cm. More strikingly, as depicted in Figure 8(g), a thin layer with reverse flow can be clearly evidenced for 0.52 cm < y < 0.61 cm at the section x = +0.62 cm. It is strongly indicated that the mean position of the separation point does occur between x = +0.45 cm and x = +0.62 cm, and the mean streamwise velocity on the air-pocket surface should be zero exactly at this mean position of separation point.

Following the flow characteristic demonstrated in Figures 8(f), (g), the distributions of mean streamwise velocity measured beneath the air pocket at three sections of x = +1.10 cm, +1.42 cm, and +1.55 cm are presented, respectively, in Figures 8(h)–(j). The thickness and negative maximum velocity within the reverse flow region are both found to be larger as the streamwise position increases from x = +0.62 cm (see Figure 8(f)) to x = +1.55 cm (see Figure 8(j)). Fairly prominent velocity gradient and shear layer exist beneath the position where the zero velocity occurs right at the lower edge of the reverse flow region. Note that the mean streamwise velocity measured nearly on the surface of air pocket takes a negative, but rather small value, due to the slippery surface of air pocket. As seen finally in Figures 8(k), (l), it is found that the thickness of reverse flow region becomes larger and the negative maximum velocity gets smaller as compared with those shown in Figures 8(h)–(j). This is due to the fact that the expansion of the shear layer and the curving surface convergent to the pipe top-wall. In addition, evident velocity gradient can be also observed especially below the lower edge of the reverse flow region where zero velocity takes place.

5 Conclusions

In this paper, the characteristics of water flow field, in the plane of symmetry, around a stationary air pocket adhered to the inner top-wall of a horizontal pipe (with flows showing fully developed turbulent boundary layer) have been demonstrated experimentally. Flow visualization technique and high-speed particle image velocimetry have been used in the experiments. The Reynolds number R_e of the pipe flow was kept at 17,100. The volume of air pocket tested was varied from 1.0 ml to 10.0 ml. The important findings of this study can be summarized as follows:

(1) The fully developed turbulent boundary layer flow in the measuring position of interest has been accomplished easily within a short streamwise distance from the pipe inlet by using the circumferential spike-like tripping.

(2) For a *horizontal* pipe, the maximum height and width of air pocket vary little as air-pocket volume being approximately larger than 2.0 ml. The air-pocket length, however, increases approximately linearly with the increase in the air-pocket volume ranging from 0 to 10.0 ml. On other words, the increase of air-pocket volume has the prominent influence on the elongation of air-pocket and is nearly without the effect on the maximum height and width of air-pocket.

(3) Based on flow visualization tests and velocity measurements using HSPIV, the water flow field around the air pocket can be mainly classified as: the horseshoe vortex taking place upstream of the air pocket and fairly near the inner top-wall of the pipe; a flow regime including both the *stagnation point* on the air-pocket surface (where the water flow bifurcates) and the *separation point* occurring at a location downstream of the stagnation point and on the air-pocket surface (where the water particle moves away from the air-pocket surface); the formation of the shear layer with a reverse flow region inside and being extended to the surface of air pocket; and the slippery motion of water particle moving from the trailing edge back to the separation point on the air-pocket surface in which the traditional non-slip condition is no longer applied.

(4) From the flow visualization pictures and HSPIV measurements results with close-up view of the instantaneous and mean flow field obtained very near the pipe top-wall and upstream of the air pocket, the instantaneous position of the core of horseshoe vortex is witnessed to change mainly with the streamwise position, but little with the transverse height, indicating the core of horseshoe vortex moves upstream and downstream randomly with respective to the mean location of the horseshoe-vortex core.

(5) The distributions of mean streamwise velocity measured in the shear layer, $u(y)$, beneath the air pocket have been subsequently presented and strongly shown that the representative shear layer thickness increases with increase of the streamwise distance x.

References

[1] E. E. Zukoski, "Influence of viscosity, surface tension, and inclination angle on motion of long bubbles in closed tubes." Journal of Fluid Mechanics, 25(4), 1966, 821-837.

[2] K. H. Bendiksen, "An experimental investigation of the motion of long bubbles in inclined tubes." International Journal of Multiphase Flow, 10(4), 1984, 467-483.

[3] C. S. Lauchlan, M. Escarameia, R. W. P. May, R. Burrows, and C. Gahan, "Air in pipelines – a literature review." Report SR 649, Rev. 2.0, HR Wallingford, 2005.

[4] H. T. Falvey, "Air-water flow in hydraulic systems, Engineering Monograph No. 41, Bureau of Reclamation, USA, 1980.

[5] S. Z. Rouhani and M. S. Sohal, "Two-phase flow patterns: A review of research results." Progress in Nuclear Energy, 11(3), 1983, 219-259.

[6] M. J. Little, "Air in pipelines." Proceedings of the 4th International Conference on Marine Waste Water Disposal and Marine Environment, Antalya, 2006.

[7] M. Wickenhauser and C. R. Kriewitz, "Air-water flow in downward inclined large pipes." Proceedings of the 33rd IAHR Congress on Water Engineering for a Sustainable Environment, 2009, 5354-5361.
[8] T. Liu and J. Yang, "Experiments of air-pocket movement in an 18.2° downward 240-mm conduit." Procedia Engineering, 2012 International Conference on Modern Hydraulic Engineering, 2012.
[9] O. P. Estrada, "Investigation on the effects of entrained air in pipelines." Ph. D. Thesis, Institute of Hydraulic Engineering, the University of Stuttgart, 2007.
[10] J. Dath and M. Mathiesen, "Pre-study of hydraulic design: Inventory and comprehensive evaluation of bottom outlet in Swedish dams." SWECO VBB, Stockholm, 2007.
[11] S. Glauser and M. Wickenhauser, "Bubble movement in downward-inclined pipes." Journal of Hydraulic Engineering, ASCE, 135(11), 2009, 1012-1015.
[12] M. J. Little, "Air transport in water and effluent pipelines." Proceedings of the 2nd International Conference on Marine Waste Water Discharges, Istanbul, 2002.
[13] C. Lin, W. Y. Huang, S. C. Hsieh, and K. A. Chang, "Experimental study on mean velocity characteristics of flow over vertical drop." Journal of Hydraulic Research, IAHR, 45(1), 2007, pp. 33 ~ 42.
[14] C. Lin, W. Y. Hsieh, S. C. Hsieh, and K. A. Chang, "Reply to the Discussion of "Experimental study on mean velocity characteristics of flow over vertical drop." Journal of Hydraulic Research, IAHR, 46(3), 2008, pp. 424-428.
[15] C. Lin, W. Y. Hsieh, S. C. Hsieh, S. S. Lin, and S. Dey, "Flow characteristics around a circular cylinder placed horizontally above a plane boundary." Journal of Engineering Mechanics, ASCE, 135(7), 2009, pp. 697-716.
[16] C. Lin, M. J. Kao, S. C. Hsieh, L. F. Lo, and R. V. Raikar, "On the flow structures under a partially inundated bridge deck." Journal of Mechanics, 28(1), 2012a, pp. 191-207.
[17] C. Lin, W. J. Lin, S. C. Hsieh, S. H. Chou, and R. V. Raikar, "Velocity and turbulence characteristics of skimming flow over a vertical drop without end sill." Journal of Mechanics, 28(4), 2012b, 607-626.